

Uptake Measurements of Ethanol on Ice Surfaces and on Supercooled Aqueous Solutions Doped with Nitric Acid between 213 and 243 K

M. Kerbrat, S. Le Calvé,* and Ph. Mirabel

Centre de Géochimie de la Surface / CNRS and Université Louis Pasteur, 1 rue Blessig, F-67084 Strasbourg cedex, France

Received: June 6, 2006; In Final Form: September 27, 2006

Uptake of ethanol either on pure frozen ice surfaces or supercooled solutions doped with HNO₃ (0.63 and 2.49 wt %) has been investigated using a coated wall flow tube coupled to a mass spectrometric detection. The experiments were conducted over the temperature range of 213–243 K. Uptake of ethanol on these surfaces was always found to be totally reversible whatever were the experimental conditions. The number of ethanol molecules adsorbed per surface unit was conventionally plotted as a function of ethanol concentration in the gas phase and subsequently analyzed using Langmuir's model. The amount of ethanol molecules taken up on nitric acid doped-ice surfaces was found to increase largely with increasing nitric acid concentrations. For example at 223 K, and for an ethanol gas-phase concentration of 1×10^{13} molecules cm³, the number of adsorbed molecules are (in units of molecules cm⁻²): $\sim 1.3 \times 10^{14}$ on pure ice; $\sim 1.4 \times 10^{15}$ on ice doped with HNO₃ 0.63 wt %; $\sim 7.5 \times 10^{15}$ on ice doped with HNO₃, 2.49 wt %, i.e. 60 times larger than on pure ice. Since, according to the shape of the isotherms, the adsorption did not proceed beyond monolayer coverage, the enormous increase of ethanol uptake was explained by considering its dissolution in either a supercooled liquid layer ($T < 230$ K) or a liquid solution ($T > 230$ K). The formation of both was indeed favored by the presence of the HNO₃. Our experimental results suggest that the amount of ethanol dissolved in such supercooled solutions follows Henry's law and that the Henry's law constants at low temperatures, i.e., 223–243 K, can be estimated by extrapolation from higher temperatures. Such supercooled solutions which exist in the troposphere either in deep convective clouds or in mixed clouds for temperature above 233 K, might be responsible for the scavenging of large amounts of soluble species, such as nitric and sulfuric acids, oxygenated VOCs including alcohols, carboxylic acids, and formaldehyde.

Introduction

The upper troposphere (UT) is characterized by its low temperatures ranging from about 188 to 233 K and by the presence of cirrus clouds covering a substantial portion (up to 25%) of the earth's surface.¹ Cirrus clouds are formed in the troposphere at altitudes of 4–15 km where they can modify both the incoming solar radiation and the outgoing terrestrial infrared radiation and thus influence climate.

Below 233 K, clouds are predominantly composed of ice crystals with number densities in the range 0.001–50 cm⁻³.^{1,2} However, above 233 K clouds composed of supercooled liquid water droplets have also been observed either in mixed clouds containing both ice crystals and supercooled droplets³ or in deep convective clouds where most of the condensed water remained liquid down to 235 K with densities up to 1.8 g m⁻³.⁴

It has been shown by model calculation^{5–7} that the presence of pollutants, such as nitric acid, may substantially modify supercooled cirrus formation at temperature above 233 K, affecting the size and number concentrations of the droplets. This in turns may have considerable climatic effects. Tropospheric mixing ratios of nitric acid vary typically between 0.1 and 2.0 ppb for altitude range of 5–13 km,⁵ i.e. in both free and upper troposphere. The partitioning of nitric acid in cirrus clouds is still not well understood, although it is an important

parameter to understand the vertical redistribution of HNO₃ in the upper troposphere.⁶ Up to now, it seems that the adsorption on the surface of ice particles is not the only process to be considered to models the scavenging of HNO₃ by clouds particles⁶ and recent studies^{6–8} have also considered the dissolution of nitric acid in liquid aerosol particles. The model of Krämer and co-workers⁶ results in concentration of HNO₃ in ternary (HNO₃–H₂SO₄–H₂O) and quaternary (NH₃–HNO₃–H₂SO₄–H₂O) solutions ranging respectively from 0.04 to 17 wt % and 1.2 to 41 wt % for temperatures between 213 and 223 K, relative humidity between 100 and 160%, and initial gaseous HNO₃ mixing ratio between 0.05 and 1.7 ppb.

Vertical advective transport influences the oxidation capacity in the troposphere and therefore the concentration and vertical distribution of trace gases. Deep convection can rapidly transport anthropogenic pollutants such as NO_x, VOCs and HO_x precursors from the planetary boundary layer (PBL) into the upper troposphere,⁹ where they can participate to the photochemistry and modify ozone concentration. During the convection, soluble gas pollutants including nitric acid are likely scavenged by supercooled droplets contained in polluted convective air masses. When ice particles are then forming, HNO₃ and other soluble species contained in those particles that freeze are retained in the bulk of these new ice crystals^{6,8} until they evaporate once in the UT.

As a consequence of convection, Laaksonen et al.⁸ observed correlated high mixing ratios of both acetone and nitric acid in

* Corresponding author. Fax: +33-(0)3-90-24-04-02. E-mail: slecalve@illite.u-strasbg.fr.

the UT (see their Figure 2) suggesting that air masses had recent contact with the polluted PBL. The presence of oxygenated volatile organic compounds (VOCs) such as alcohols, ketones, and carboxylic acids in the UT is also well established.^{10–13} Among the alcohols encountered in either the Troposphere or the UT, methanol is the most abundant with concentrations ranging typically between 400 and 900 pptv^{10,13} while ethanol levels reach up to 50 pptv in the UT.¹⁰

Recent studies have focused on the adsorption of oxygenated VOCs on pure ice surfaces^{14–19} and have highlighted that the adsorption of such species on pure ice is a minor process so that only gas-phase reactions have to be considered to describe their chemistry in the UT.

If the amount of adsorbed organic molecules is always limited on pure ice, Journet et al.²⁰ have shown that acetone quantities taken up by nitric acid doped-ice surfaces were 1 or 2 orders of magnitude higher than those obtained on pure ice. Such an amount of acetone molecules, up to 50 times higher than its monolayer capacity on pure ice surfaces, cannot be adsorbed on the ice surface and therefore, these molecules are most likely dissolved in a supercooled liquid layer that forms the outermost surface of the ice crystals.

This study aims to examine the interaction of ethanol with nitric acid supercooled aqueous solutions mimicking supercooled cloud droplets, at temperatures relevant for supercooled cirrus clouds, i.e., around 233 K, and to compare the surface coverage of ethanol on these HNO₃ supercooled solutions with those obtained on pure ice by Peybernès et al.¹⁴ with the same experimental setup. As the temperature range of this previous study was limited to 193–223 K, a first part of this work was to extend this range to higher temperatures, i.e., 233 and 243 K. Nitric acid is easily scavenged by clouds to form supercooled solution droplets. It is therefore important to study the interaction of ethanol with nitric acid doped supercooled solutions. This was done from 213 to 243 K under realistic nitric acid concentrations, i.e., 0.63 wt % HNO₃ (0.1 N) and 2.49 wt % HNO₃ (0.4 N). The concentrations used in our study are therefore similar to those found in a ternary solution if the initial HNO₃ gas phase mixing ratio is 0.26 ppb and the relative humidity in the range 100–130%. Such conditions are very close to those measured by Gao and co-workers²¹ in a cirrus cloud. The low HNO₃ percentages in particles are also consistent with those reported by Lin and Tabazadeh (in 2001) for a broad range of upper tropospheric conditions.²² The vapor pressure of HNO₃ over our adsorbent was calculated using the equation of Taleb et al.²³ It ranges from 1.3×10^{-10} to 1.6×10^{-7} Torr which corresponds to a mixing ratio of respectively 0.7 and 800 ppt (at a total atmospheric pressure of 0.27 atm) which is in agreement with the findings of Gao and co-workers.²¹

To our knowledge, this work is the first to report uptake of ethanol on nitric acid supercooled solutions. Our experimental data were then used to estimate the partitioning of oxygenated VOCs such as acetone and ethanol between the gas phase and the supercooled liquid droplets in a typical convective cloud.

Experimental Section

The uptake of ethanol on ice surfaces and on supercooled aqueous solutions was studied using a vertical coated wall flow tube coupled to a mass spectrometer, already described elsewhere.^{14,15,20} We will therefore provide only a brief summary of its principle of operation. The apparatus, which is shown in Figure 1, has a double jacket to allow the system to be operated at low temperature. The cooling fluid was circulated in the inner jacket from a cooler/circulator (Huber, Unistat 385) while

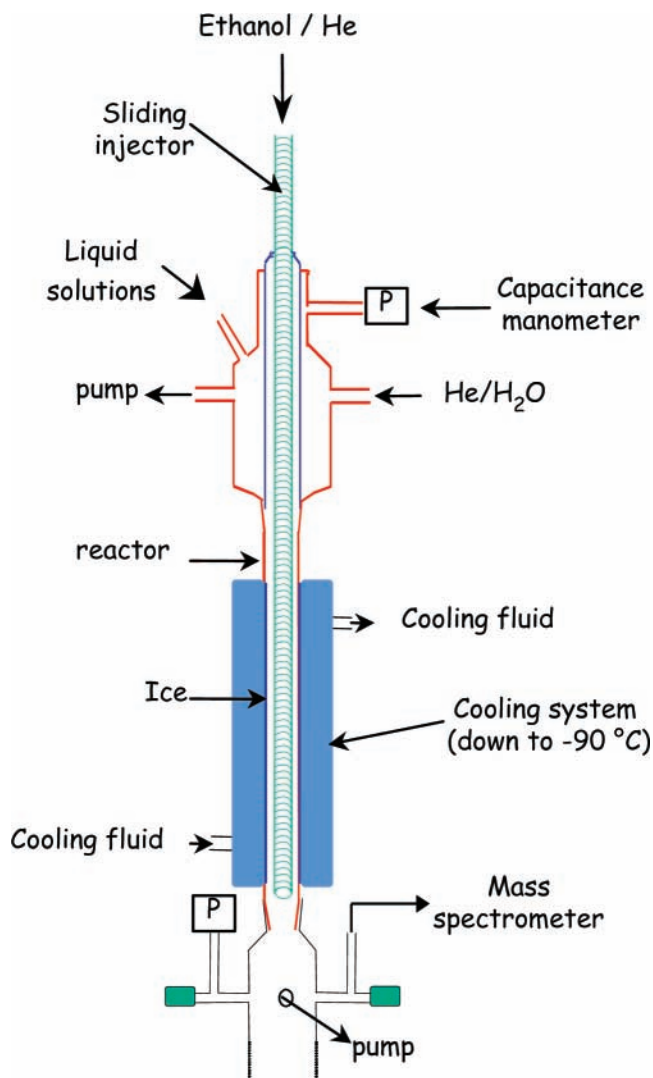


Figure 1. Schematic illustration of the vertical coated wall flow tube.

vacuum was maintained in the outer jacket for thermal insulation. The temperature of the flow tube could be cooled down and regulated between 193 and 243 K.

The jacketed flow tube was approximately 40 cm in length with an internal diameter of 2.8 cm. The ice surface was prepared by totally wetting, with either Milli-Q water (18 MΩ cm) or solutions containing HNO₃ (0.63 and 2.49 wt %), the inner wall of the flow tube that was precooled to 255 K for pure water and 260 K for acid solutions. The viscous aqueous film was then cooled down to the desired temperature over a period of 10–15 min. The thickness of the ice film was estimated between 40 and 100 μm by weighting the resulting liquid water, when the ice film was melted at the end of the experiment.

The helium carrier gas (UHP certified to >99.9995% from Alphagaz) was used without further purification. During the experiment, water vapor was added to the main He flow in order to provide a partial pressure of water, equal to the vapor pressure of water over the ice film and therefore inhibit net evaporation of this film. The resulting humidified helium flow was injected at the upstream end of the flow reactor.

Ethanol (99.8%) purchased from Carlo Erba was further purified before being used by repeated freeze, pump, and thaw cycles as well as by fractional distillation. To perform an experiment, ethanol was premixed with helium in a 10 L glass light-tight bulb to form 5.1×10^{-3} to 5.4×10^{-2} % mixtures,

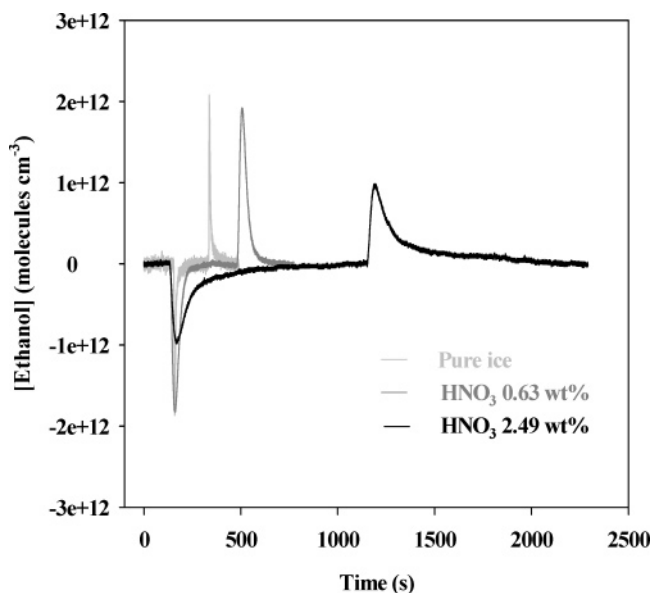


Figure 2. Relative ethanol concentrations in the gas phase as a function of time during the adsorption of ethanol on different ice surfaces at 223 K (with $[\text{Ethanol}]_{\text{gas phase}} = 3.38, 3.49,$ and 2.90×10^{12} molecules cm^{-3} for respectively pure ice, HNO_3 0.63 wt % and HNO_3 2.49 wt %).

at a total pressure of ~ 750 – 1200 Torr. The mixture containing ethanol was injected into the flow tube reactor via a sliding injector (Figure 1) that allows changing the exposed ice film surface (30 – 230 cm^2). The injector was jacketed, and a heating tape was wound up in the jacket, to ensure a gentle heating of the injector.¹⁵

All the gases flowed into the reactor through Teflon tubing. The gas mixture containing ethanol and water vapor diluted in helium was flowed through the reactor with a linear velocity ranging between 30 and 100 cm s^{-1} . Concentrations of ethanol in the gas phase were calculated from their mass flow rates, temperature and pressure in the flow tube. All the flow rates were controlled and measured with calibrated mass flowmeters (Millipore, 2900 series). The pressure that ranged between 1.9 and 2.9 Torr, was measured with two capacitance manometers (Edwards, 622 Barocel range 0 – 100 Torr and Keller, PAA-41 range 0 – 76 Torr) connected at the top and bottom of the flow tube. Under our experimental conditions, the mixing time τ_{mix} between ethanol flow and the main He flow was lower than 2 ms ²⁴ which corresponds to a mixing length smaller than 0.3 cm.

The gas stream coming out of the flow tube was analyzed using a differentially pumped mass quadrupole spectrometer Pfeiffer Vacuum QMS. Ethanol was monitored at the main fragment ion $\text{CH}_3\text{CH}_2\text{O}^+$ peak at $m/z = 45$ amu using a temporal resolution of 100 ms, an ionization energy of 70 eV and an emission current of 1000 μA .

Results and Discussion

Uptake experiments were performed by first establishing a highly stable flow of ethanol in the injector, this injector being positioned past the end of ice film. The injector was then moved quickly to an upstream position so that the ice film was exposed to ethanol. The uptake of ethanol on the ice film leads to a drop of signal as shown in Figure 2. After a time scale ranging from a few seconds to several minutes depending on the investigated ice surface, the ice surface was then saturated and the MS-signal returned to its initial level. When the injector was pushed back, the ethanol desorbed from the ice surface and

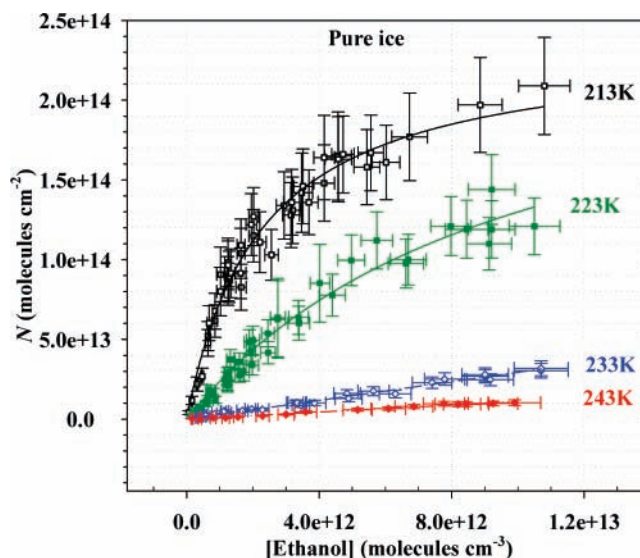


Figure 3. Adsorption isotherms of ethanol on pure ice surfaces. Isotherms at 213 and 223 K have been obtained by Peybernès et al.¹⁵ and extended in this work while those at 233 and 243 K have been exclusively measured in this work.

the signal increased and then again returned to its initial level. Similar experiments were conducted for various ice surfaces (pure ice or doped-ice surfaces) over a temperature range 213 – 243 K and for gas-phase concentrations varying from 8.8×10^{10} to 1.9×10^{13} molecules cm^{-3} .

Adsorption on Pure Ice Surfaces. This study extends to higher temperature (233 and 243 K) the previous work of Peybernès et al.¹⁵ made on pure ice surfaces between 193 and 223 K. However, several data points were also collected at 213 and 223 K to check the reproducibility of our previous results.

Surface Coverage. The number of ethanol molecules adsorbed N_{ads} on the ice surface was determined from the integrated area of the adsorption peak (in molecule s cm^{-3}) and the total flow rate in the flow tube ($\text{cm}^3 \text{s}^{-1}$). The surface coverage N (in molecules cm^{-2}) of ethanol was then calculated from the geometric exposed ice surface area S_{ice} (in cm^2) according to $N = N_{\text{ads}}/S_{\text{ice}}$. The experiments were performed several times, using newly generated ice surfaces in order to ensure the reproducibility of the data.

Surface coverage N vs gas-phase concentrations has been plotted in Figures 3, for four temperatures: 213 , 223 , 233 , and 243 K. The relative errors on the gas-phase concentrations which range between 7 and 20% (horizontal error bars in this figure) have been calculated from the possible uncertainties on each flow, total pressure etc. The quoted errors on N (vertical error bars) arise from uncertainties made on the total flow rate, exposed ice area and concentrations in the gas phase. They also include a systematic 2% error that corresponds to the error on the integrated area of adsorption peaks. These resulting errors on N vary between 14 and 30% .

Langmuir Isotherms. Langmuir's theory, which main assumption is that adsorption cannot proceed beyond monolayer coverage, was used to analyze our experimental data. According to this theory, the number of molecules adsorbed per unit area of ice surface is related to the concentration of ethanol in the gas phase. Equation 1 states this dependence:

$$\theta = \frac{N}{N_M} = \frac{K_{\text{ads}}(T)[\text{Ethanol}]_{\text{gas}}}{1 + K_{\text{ads}}(T)[\text{Ethanol}]_{\text{gas}}} \quad (1)$$

TABLE 1: Values of the Monolayer Capacity N_M and of the Langmuir Constant K_{ads} at 213 and 223 K Obtained with the Langmuir Model, Where Values of $N_M \times K_{\text{ads}}$ at 233 and 243 K Have Been Determined from the Slopes of the Plots of N vs Ethanol Concentration (see Eq 2) and the Quoted Errors Correspond to 2σ Level + 5% (see Text).

T (K)	N_M^a ($\times 10^{14}$)	K_{ads}^b ($\times 10^{-13}$)	$N_M \times K_{\text{ads}}$ (cm)	model
213	2.37 (± 0.27)	4.48 (± 0.72)		Langmuir
223	2.58 (± 0.62)	1.01 (± 0.32)		Langmuir
233		0.12 (± 0.04) ^c	2.94 (± 0.23)	linear plot
243		0.04 (± 0.01) ^c	1.11 (± 0.09)	linear plot

^a In units of molecules cm^{-2} . ^b In units of $\text{cm}^3 \text{molécule}^{-1}$. ^c Determined by assuming that $N_M = 2.5 \times 10^{14}$ molecules cm^{-2} is constant between 213 and 243 K.

where θ is the fractional coverage, N_M is the monolayer capacity (in molecules cm^{-2}), and $K_{\text{ads}}(T)$ is the temperature dependent adsorption constant that describes partitioning between adsorbed and non-adsorbed molecules ($\text{cm}^3 \text{molecule}^{-1}$).

Figure 3 summarizes our experimental adsorption isotherms, together with those of Peybernès et al.¹⁵ Only the data collected at 213 and 223 K by Peybernès et al.¹⁵ were used for the Langmuir's analysis. Indeed, for temperature below 213 K, the Langmuir's model is no more relevant to describe the adsorption phenomena.²⁵ For these two temperatures, data were fitted according to eq 1 considering both N_M and K_{ads} as free parameters. The resulting values for the Langmuir constants K_{ads} and monolayer capacities N_M are reported in Table 1. The errors bars are given at 2σ level and include experimental error that can be estimated to approximately 5%. Since no significant variation of N_M with temperature was found between 213 and 223 K an average value $N_M = (2.5 \pm 0.7) \times 10^{14}$ molecules cm^{-2} has been calculated.

At 233 and 243 K, $K_{\text{ads}}(T)[\text{Ethanol}]_{\text{gas}} \ll 1$ in eq 1 and N increases linearly with the ethanol concentration with a slope $N_M K_{\text{ads}}(T)$ according to

$$\theta = \frac{N}{N_M} = K_{\text{ads}}(T)[\text{Ethanol}]_{\text{gas}} \quad (2)$$

At these temperatures neither N_M nor $K_{\text{ads}}(T)$ can be directly derived. However, assuming that N_M does not vary between 213 and 243 K allows us to estimate $K_{\text{ads}}(T)$ at 233 and 243 K (see Table 1).

The temperature dependence of $K_{\text{ads}}(T)$ between 213 and 243 K was used to determine the adsorption enthalpy ΔH_{ads} of ethanol on pure ice, according to

$$\ln K_{\text{ads}} = \ln A - \frac{\Delta H_{\text{ads}}}{RT} \quad (3)$$

where A is a constant and R is the perfect gas constant.

As expected, the plot of $\ln K_{\text{ads}}$ vs $1/T$ is linear for the temperature range 213–243 K. This is shown in Figure 4 where we have plotted the results of the present study together with those obtained by Peybernès (in 2003)²⁵ and Sokolov and Abbatt (in 2002).¹⁹ It can be seen here that for temperature below 213 K, values start to deviate due to the irrelevant description of the adsorption via the Langmuir's model.²⁵ Nonetheless, the BET model can be successfully used to analysis data obtained at low temperatures.¹⁴ The resulting adsorption enthalpy of ethanol on ice between 213 and 243 K, obtained by linear weighted least-squares fitting, is $\Delta H_{\text{ads}} = -68 \pm 15 \text{ kJ mol}^{-1}$ (the quoted errors are given at 2σ level + 5%).

Comparison with Previous Studies. Our value $N_M = (2.5 \pm 0.7) \times 10^{14}$ molecules cm^{-2} is consistent with those reported

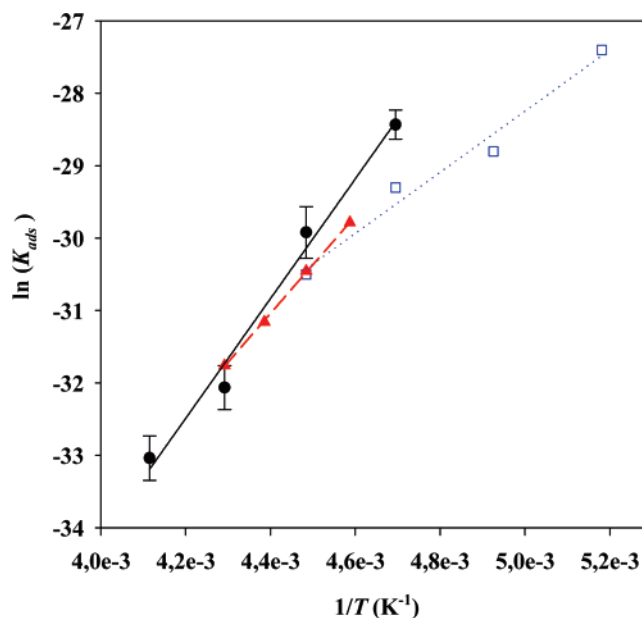


Figure 4. Plot of K_{ads} as a function of $1/T$. The enthalpy associated with the adsorption process is derived from the slope according to the eq 3. Our values (●) are here compared with those obtained by (□) Peybernès²⁵ (in 2003) and (▲) Sokolov and Abbatt¹⁹ (in 2002).

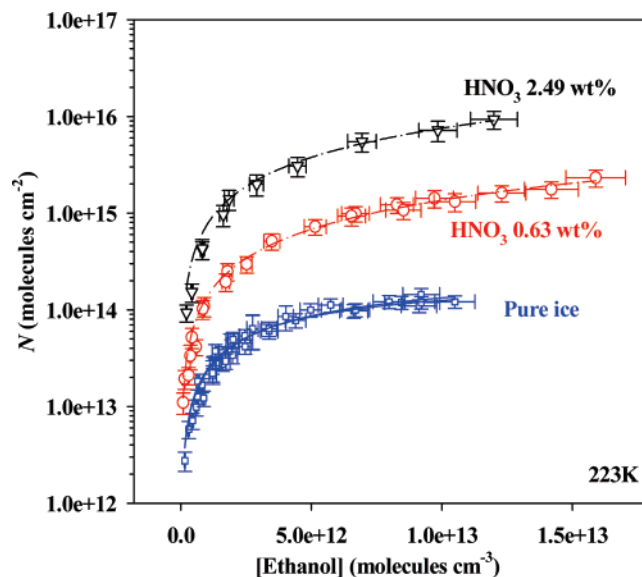


Figure 5. Adsorption isotherms on different types of ice at 223 K (Logarithmic scale).

in previous studies: $N_M = 2.9 \times 10^{14}$ for T in the range 218–233 K¹⁹ and $N_M = (2.8 \pm 0.8) \times 10^{14}$ for T in the range 193–223 K.¹⁴ Similarly, our value of the adsorption enthalpy $\Delta H_{\text{ads}} = -68 \pm 15 \text{ kJ mol}^{-1}$ compares favorably with the determinations of Sokolov and Abbatt¹⁹ ($\Delta H_{\text{ads}} = -61.8 \pm 3.3 \text{ kJ mol}^{-1}$) and of Peybernès et al.¹⁴ ($\Delta H_{\text{ads}} = -57 \pm 8 \text{ kJ mol}^{-1}$). Note that the value obtained by Peybernès et al. (2004) was derived from BET analysis.¹⁴

Adsorption on Ice Surfaces Doped with HNO_3 . Experiments were conducted on ice films doped with HNO_3 (0.1 and 0.4 N which correspond to 0.63 and 2.49 wt % of HNO_3) at temperatures ranging from 213 to 243 K. These temperatures and nitric acid concentrations were chosen to mimic the conditions which have been encountered in cirrus clouds.^{21,26,27} Consequently, for some temperatures (233 and 243 K) we were operating in the liquid–solid domain of the equilibrium phase

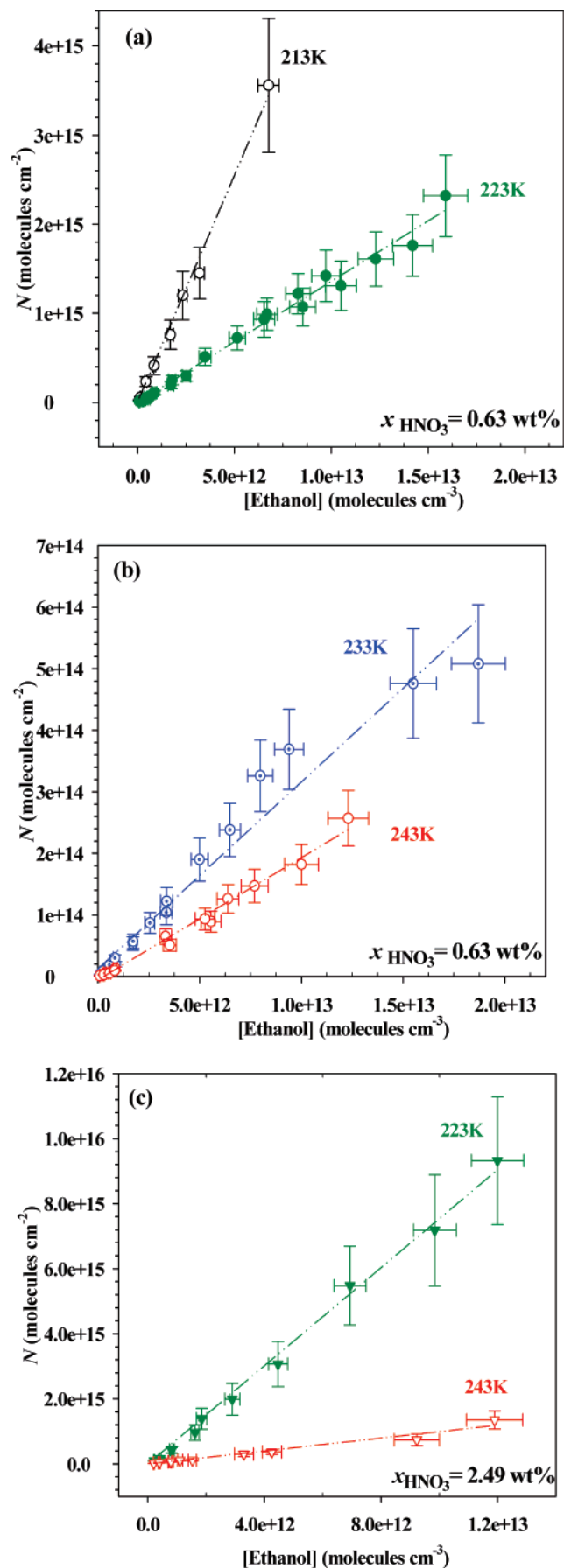


Figure 6. Linear adsorption isotherms of ethanol on both type of nitric acid doped-ice (a) on 0.63 wt % nitric acid doped-ice at 213 and 223 K (b) and at 233 and 243 K, (c) on 2.49 wt % nitric acid doped-ice at 223 and 243 K.

TABLE 2: Values of the Pseudo Henry's Law Constant H^* (in $\text{Mol L}^{-1} \text{atm}^{-1}$) Calculated According to Eq 5, Where Two Thicknesses Are Used for the "Ice" Films (40 and 100 μm) and the Quoted Errors Correspond to 2σ Level + 5% (See Text)

HNO_3 doped-ice surface (wt %)	T (K)	e (μm)	$N_M \times K_{\text{ads}}$ (cm)	H^*	H^* (mean value)
0.63	213	40	509 (± 48)	2.91×10^5	$2.04 (\pm 0.9) \times 10^5$
		100		1.16×10^5	
	223	40	135 (± 12)	7.38×10^4	$5.16 (\pm 2.3) \times 10^4$
		100		2.95×10^4	
	233	40	32 (± 4)	1.67×10^4	$1.17 (\pm 0.6) \times 10^4$
		100		6.70×10^3	
243	40	19 (± 2)	9.53×10^3	$6.67 (\pm 3.0) \times 10^3$	
	100		3.81×10^3		
2.49	223	40	753 (± 63)	1.13×10^5	$7.91 (\pm 3.5) \times 10^4$
		100		4.51×10^4	
	243	40	99 (± 15)	1.38×10^4	$9.66 (\pm 4.2) \times 10^3$
		100		5.52×10^3	

diagram of the $\text{HNO}_3/\text{H}_2\text{O}$ system,²⁸ since the solidus lies at 230–231 K in this region of the diagram. The use of the lever rule shows that for 2.49 wt % HNO_3 solution and for T in the range 233–243 K, 90–92% of the mixture is solid (pure ice). These numbers translate to 97.5–98% for 0.63 wt % solutions.

The adsorption peaks which, on pure ice extended over a few seconds, spread out over more than 30 min for ice doped with HNO_3 (2.49 wt %) as shown in Figure 2. Note that adsorption of ethanol was always reversible under our experimental conditions whatever the concentration of HNO_3 . This observation is consistent with the fact that no product has been detected suggesting that no reaction occurred on the ice surface. In addition, pH-metric analysis were performed on the liquid resulting from the melting of the ice film after a series of experiments and no significant loss or increases in acid concentration were detected.

The number of ethanol molecules taken up on the ice surfaces doped with HNO_3 increased by one or two order of magnitudes compared to pure ice surfaces and, as it can be seen in Figure 5, the surface coverage increases with the nitric acid concentration. At 223 K for example, temperature below the solidus line, and for an ethanol gas-phase concentration of 1×10^{13} molecules cm^{-3} , the number of adsorbed molecules are (in units of molecules cm^{-2}): $\sim 1.3 \times 10^{14}$ (pure ice); $\sim 1.4 \times 10^{15}$ (HNO_3 0.63 wt %); $\sim 7.5 \times 10^{15}$ (HNO_3 2.49 wt %). With a 2.49 wt % acid concentration, the number of adsorbed molecules is then 60 times more important than on pure ice. Even at the lowest HNO_3 concentrations, the amount of adsorbed molecules is 1 order of magnitude higher than the one determined on pure ice. Similar behaviors can be observed at 213, 233, or 243 K.

The huge quantities of ethanol taken up by nitric acid doped-ice surfaces can be explained in two different ways. We have seen above that the number of molecules taken up on a doped surface can be 60 times higher than on pure ice. Therefore, one could imagine that the ethanol molecules are adsorbed in multilayers. However, the shapes of our experimental isotherms, which tend to level off at high ethanol gas-phase concentrations, are not consistent with those reported in Brunauer's classification²⁹ for multilayer coverages.

The second possibility may reside in the dissolution of ethanol in a liquid phase or in a supercooled liquid layer. At 233 and 243 K, the temperature is, as noted previously, above the solidus temperature and therefore a liquid solution exists, which

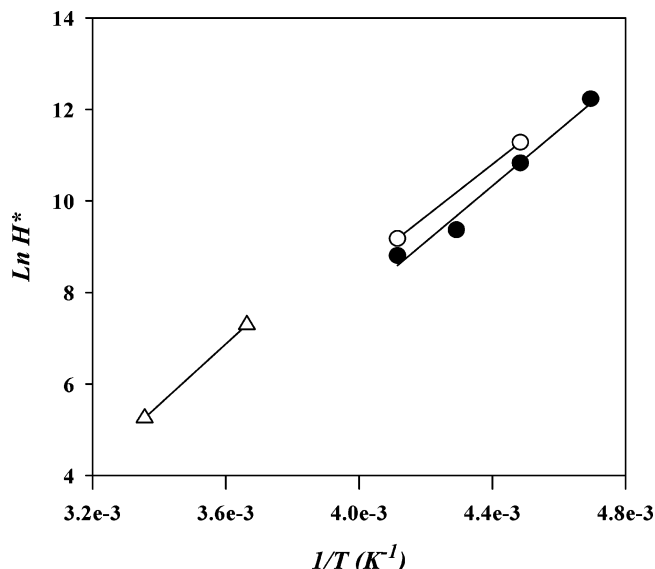


Figure 7. Plot of $\ln H^*$ as a function of $1/T$. The resulting values of our measurements on 0.63 wt % (●) and 2.49 wt % (○) nitric acid doped-surface are compared with the values of Snider and Dawson³⁰ (in 1985) (△) obtained for pure liquid water surfaces.

TABLE 3: Values of the Pseudo Henry's Law Constant H^* (in Units of $\text{mol L}^{-1} \text{atm}^{-1}$) and of Atmospheric Aqueous Fraction f_{aq} for Various Oxygenated VOCs at Supercooled Cloud Temperature of 233 K, Where H^* Values Have Been Estimated from Extrapolation of the Henry's Law Established at Higher Temperature as Suggested by Our Results.

compound	$H(298\text{K})$	$-(d(\ln H))/(d(1/T))$	$H^*(233\text{K})$	$f_{\text{aq}}(233\text{K})$
methanol	220 ^a	5200 ^a	9.16×10^4	0.76
ethanol	190 ^a	6600 ^a	2.86×10^4	0.50
acetone	30 ^b	4600 ^b	2.22×10^3	0.07
formic acid	5400 ^b	5700 ^b	1.12×10^6	0.97
acetic acid	5500 ^b	6300 ^b	2.00×10^6	0.98
formaldehyde	3200 ^b	6800 ^b	1.86×10^6	0.98

^a Snider and Dawson (1985).³⁰ ^b Staudinger and Roberts (1996).³³

represents about 2–3% and 8–10% by weight for 0.63 and 2.49 wt % solutions respectively. From the phase diagram²⁸ the composition of this solution is about 27% (243 K) and 31% (233 K) nitric acid by weight. The enhanced uptake for ethanol at these temperatures most likely results because absorption into a liquid (where diffusion is favored compared to a solid) is more efficient than adsorption onto a solid.

For the lowest two temperatures, 213 and 223, which are below the solidus curve, some degrees of supercooling cannot be excluded and in such a case, the composition of the solution would be close to 31% HNO_3 by weight. In addition the presence of ethanol, which is known to strongly depress the freezing point of water, will also favor the supercooling of the solution.

The presence of a liquid solution is consistent with the adsorption/desorption cycles observed in Figure 2. The cycles are much longer for experiments performed on nitric acid doped-ice surfaces compare to those conducted on pure ice films. When the liquid-phase exists, the kinetic of uptake and desorption could be effectively driven by the diffusion rate of ethanol in the solution. As shown in Figure 2, we can also note that this time of the adsorption/desorption processes increased with increasing of nitric acid concentration, which correspond to an increase of the amount of solution.

Ethanol could then dissolve in the liquid solution according to Henry's law equilibrium:

$$H = \frac{[\text{Ethanol}]_{\text{liq}}}{P_{\text{Ethanol}}} \quad (4)$$

where H is the Henry's law constant conventionally expressed in $\text{mol L}^{-1} \text{atm}^{-1}$, $[\text{Ethanol}]_{\text{liq}}$ is the ethanol concentration in the liquid (in mol L^{-1}), P_{Ethanol} is the partial pressure of ethanol over the liquid phase (in atm).

Such a hypothesis is consistent with the fact that N first increases linearly with the gas-phase concentration of ethanol (see Figure 6). In such a case a pseudo Henry's law constant H^* can be introduced and derived by combining eq 2 and eq 4 which leads to

$$H^* = \frac{[\text{Ethanol}]_{\text{liq}}}{P_{\text{Ethanol}}} = \frac{1.013 \times 10^6 N_M K_{\text{ads}}}{epRT} \quad (5)$$

where $N_M \times K_{\text{ads}}$ is the slope of the adsorption isotherms in cm, e is the thickness of the ice film expressed in μm , p is the percentage of liquid given by the phase diagram, and R is the gas constant in $\text{J mol}^{-1} \text{K}^{-1}$.

This equation was considered to estimate H^* under our experimental conditions, and the results are shown in Table 2. Calculations were made for a film thickness of 40 or 100 μm , which are the two extreme values found by weighting the solution at the end of an experiment (see the experimental section) and p was estimated to 2.5 and 9% for 0.63 and 2.49 wt % nitric acid doped-ice surfaces, respectively.

Since the behavior of Henry's law constants as a function of temperature can be expressed with a Van't Hoff equation, $\ln H^*$ have been plotted as a function of $1/T$. As shown in Figure 7, a straight line can be fitted through the experimental data set. Although our Henry's constants refer to the partitioning of ethanol between the gas phase and a water-nitric acid solution in the liquid phase, it is tempting to compare our values of H^* to those of the usual gas/water equilibrium obtained at 298 and 273 K, i.e., 192 (± 9) and 1470 (± 90) $\text{mol L}^{-1} \text{atm}^{-1}$, respectively.³⁰ Although obtained under different conditions, the two sets of data are in very good agreement. We observe that the slopes derived from these plots lead to $6.1 (\pm 0.7) \times 10^3$ K and 5.7×10^3 K for the uptake of ethanol on 0.63 and 2.49 wt % nitric acid doped-ice, respectively are close to that of Snider and Dawson³⁰ (in 1985), i.e. 6.6×10^3 K. These observations seem to confirm the existence of a supercooled solution for the two temperatures below the solidus line.

Conclusion

The amount of VOCs scavenged by pure ice is negligible as shown in this work and in previous laboratory studies.^{14–19} Our experiments have shown that uptake of oxygenated VOCs such as acetone and ethanol on supercooled liquid solutions was much more important than that on pure ice. The corresponding dissolved amounts depend on the value of the Henry's law constant at these low temperatures, which can be estimated by extrapolation from higher temperature values, as shown in our ethanol study.

These estimated Henry's law constants can then be used to evaluate the partitioning of oxygenated VOCs between the gas and liquid phases inside a supercooled cloud at temperature close to 230–240 K. Assuming that both mass accommodation and gas diffusion do not limit the rate of gas uptake and therefore that the equilibrium between the gas and supercooled liquid

phases is rapidly reached, the fraction of A in the aqueous phases ($f_{A, \text{aq}}$) can be estimated as follows:³¹

$$f_{A, \text{aq}} = \frac{[A]_{\text{aq}}}{[A]_{\text{g}} + [A]_{\text{aq}}} = \frac{H^* R L_{\text{wc}} T}{1 + H^* R L_{\text{wc}} T} \quad (6)$$

where R is the ideal gas constant (in $\text{L atm mol}^{-1} \text{K}^{-1}$), L_{wc} the dimensionless liquid water content of the supercooled cloud, and T the cloud temperature (in K).

In situ measurements in deep convective clouds have shown that the supercooled droplets can reach a median volume diameter of $17 \mu\text{m}$ and amount to 1.8 g m^{-3} corresponding to $L_{\text{wc}} = 1.80 \times 10^{-6}$, which is approximately 1 order of magnitude higher than those usually reported for tropospheric clouds.³² On the basis of this value of L_{wc} and on the extrapolated values of H^* reported in Table 3 for various oxygenated VOCs, the calculated aqueous fraction f_{aq} at supercooled temperature of 233 K are the following: methanol, 0.76; ethanol, 0.50; acetone, 0.07; formic acid, 0.97; acetic acid, 0.98; formaldehyde, 0.98.

Such aqueous fractions suggest that most of formaldehyde, carboxylic acids and alcohols present in polluted boundary layer air might be scavenged by supercooled liquid droplets of convective clouds where they could be trapped inside after freezing at temperature lower than 233 K. These organic species could therefore be transported to the upper troposphere and participate to the chemistry and ozone destruction cycles once released in the gas phase by evaporation of ice crystals.

Acknowledgment. This work was supported by the French Ministry of Research through the LEFE/CHAT program. This is EOST Contribution No. 2007.101-UMR7517.

References and Notes

- Heymfield, A. J.; Sabin, R. M. *J. Atmos. Sci.* **1989**, *46*, 2252.
- Hoyle, C. R.; Luo, B. P.; Peter, T. *J. Atmos. Sci.* **2005**, *7*, 2568.
- Sassen, K.; Liou, K.-N.; Kinne, S.; Griffin, M. *Science* **1985**, *227*, 410.
- Rosenfeld, D.; Woodley, W. L. *Nature (London)* **2000**, *405*, 440.
- Laaksonen, A.; Hienola, J.; Kulmala, M.; Arnold, F. *Geophys. Res. Lett.* **1997**, *24*, 3009.
- Krämer, M.; Schiller, C.; Ziereis, H.; Ovarlez, J.; Bunz, H. *Tellus Ser. B, Chem. Phys. Meteorol.* **2006**, *58B*, 141.
- Kärcher, B.; Voigt, C. *Geophys. Res. Lett.* **2006**, *33*, L08806.
- Stuart, A. L.; Jacobson, M. Z. *J. Geophys. Res.* **2003**, *108*, doi: 10.1029/2001JD001408.
- Kley, K. *Science* **1997**, *276*, 1043.
- Singh, H.; Chen, Y.; Staudt, A.; Jacob, D.; Blake, D.; Heikes, B.; Snow, J. *Nature* **2001**, *410*, 1078.
- Arnold, F.; Bürger, V.; Droste-Fanke, B.; Grimm, F.; Krieger, A.; Schneider, J.; Stülp, T. *Geophys. Res. Lett.* **1997**, *24*, 3017.
- Mari, C.; Säit, C.; Jacob, D.; Ravetta, F.; Anderson, B.; Avery, M. A.; Blake, D. R.; Brune, W. H.; Faloon, I.; Gregory, G. L.; Heikes, B. G.; Sachse, G. W.; Sandholm, S. T.; Singh, H. B.; Talbot, R. W.; Tan, D.; Vay, S. *J. Geophys. Res.* **2003**, *108*–D2, 8229.
- Singh, H.; Chen, Y.; Tabazadeh, A.; Fukui, Y.; Bey, I.; Yantosca, R.; Jacob, D.; Arnold, F.; Wohlfrom, K.; Atlas, E.; Flocke, F.; Blake, D.; Heikes, B.; Snow, J.; Talbot, R.; Gregory, G.; Sachse, G.; Vay, S.; Kondo, Y. *J. Geophys. Res.* **2000**, *105*, 3 795.
- Peybernès, N.; Le Calvé, S.; Mirabel, P. *J. Chem. Phys. B* **2004**, *108*, 17425.
- Peybernès, N.; Marchand, C.; Le Calvé, S.; Mirabel, P. *Phys. Chem. Chem. Phys.* **2004**, *6*, 1277.
- Winkler, A. K.; Holmes, N. S.; Crowley, J. N. *Phys. Chem. Chem. Phys.* **2002**, *4*, 5270.
- Picaud, S.; Hoang, P. N. N.; Peybernès, N.; Le Calvé, S.; Mirabel, P. *J. Chem. Phys.* **2005**, *122*, 194707.
- Dominé, F.; Rey-Hanot, L. *Geophys. Res. Lett.* **2002**, *29*, 1873.
- Sokolov, O.; Abbatt, J. P. D. *J. Phys. Chem. A* **2002**, *106*, 775.
- Journet, E.; Le Calvé, S.; Mirabel, P. *J. Phys. Chem. B* **2005**, *109*, 14112.
- Gao, R. S.; Popp, P. J.; Fahey, D. W.; Marcy, T. P.; Herman, R. L.; Weinstock, E. M.; Baumgardner, D. G.; Garrett, T. J.; Rosenlof, K. H.; Thompson, T. L.; Bui, P. T.; Ridley, B. A.; Wofsy, S. C.; Toon, O. B.; Tolbert, M. A.; Karcher, B.; Peter, T.; Hudson, P. K.; Weinheimer, A. J.; Heymsfield, A. *J. Science* **2004**, *303*, 516.
- Lin, J.-S.; Tabazadeh, A. *J. Geophys. Res.* **2001**, *106*, 4815.
- Taleb, D. E.; Ponche, J. L.; Mirabel, P. *J. Geophys. Res.* **1996**, *101*, 25967.
- Taylor, G. *Proc. R. Soc. London* **1953**, *219*, 186.
- Peybernès, N. Etude de l'adsorption de composés organiques volatils oxygénés sur des surfaces de glace entre 193 et 223 K. Application à la chimie des nuages de la Haute Troposphère. Thèse de doctorat, Université Louis Pasteur, 2003.
- Heymsfield, A. J.; Knollenberg, R. G. *J. Atmos. Sci.* **1972**, *29*, 1358.
- Gayet, J. F.; Febvre, G.; Brogniez, G.; Chepfer, H.; Renger, W.; Wendling, P. *J. Atmos. Sci.* **1996**, *53*, 126.
- Beyer, K. D.; Hansen, A. R. *J. Phys. Chem. A* **2002**, *106*, 10275.
- Gregg, S. J.; Sing, K. S. W. *Adsorption, Surface Area and Porosity*, 2nd ed.; Academic Press Inc.: San Diego, CA, 1982.
- Snider, J. R.; Dawson, G. A. *J. Geophys. Res.* **1985**, *90*–D2, 3797.
- Seinfeld, J. H.; Pandis, S. N. *Atmospheric Chemistry and Physics*; Wiley: New York, 1998.
- Kolb, C. E.; Worsnop, D. R.; Zahniser, M. S.; Davidovits, P.; Hanson, D. R.; Ravishankara, A. R.; Keyser, L. F.; Leu, M. T.; Williams, L. R.; Molina, M. J.; Tolbert, M. A. Laboratory Studies of Atmospheric Heterogeneous Chemistry. In *Advances in Physical Chemistry Series*; Barker, J. R., Ed.; World Scientific: Singapore, 1995; Vol. 3, pp 771.
- Staudinger, J.; Roberts, P. J. *Crit. Rev. Environ. Sci. Technol.* **1996**, *26*, 205.